Numerico-Empirical Analyses of Atmospheric Diffusion Theories

ROBERT G. LAMB,[1] WEN H. CHEN AND JOHN H. SEINFELD

Department of Chemical Engineering, California Institute of Technology, Pasadena 91125

(Manuscript received 19 June 1974, in revised form 21 March 1975)

ABSTRACT

Numerico-empirical expressions for the particle displacement probability density function from which the mean concentration of material in turbulent fluid may be obtained are derived from the numerical planetary boundary layer model of Deardorff. These expressions are then used to compute profiles of the mean, cross-wind-integrated concentration of an inert pollutant issuing from a continuous point source below a stable layer. Profiles are derived for each of two conditions of atmospheric stability: $z_i/L=0$ and -4.5, where z_i is the inversion base height and L the Monin-Obukhov length. The resulting concentration profiles [referred to as the numerico-empirical (NE) profiles] are then used in two separate experiments designed to assess the adequacy of conventional atmospheric diffusion formulations.

First, the validity of the atmospheric diffusion equation is assessed by determining for each of the two stabilities cited above the profile of vertical eddy diffusivity that produces the closest fit of the mean concentration predicted by the atmospheric diffusion equation with the NE profiles.

Second, comparisons are made between the NE profiles and the corresponding concentration distributions predicted by the Gaussian plume formula with Pasquill-Gifford dispersion parameters, and the Gaussian puff equation with McElroy-Pooler travel-time-dependent dispersion parameters.

1. Introduction

The techniques for describing the statistical properties of the concentrations of marked particles, such as air pollutants, in a turbulent fluid can be divided into two broad categories—Eulerian and Lagrangian. The starting point of the Eulerian methods is the mass continuity equation (ignoring molecular diffusion)

$$\frac{\partial c}{\partial t}+\frac{\partial}{\partial x_i}u_i c=S, \tag{1}$$

where c denotes the particle concentration, u_i represents the ith component of the instantaneous (Eulerian) fluid velocity, and S is a known function describing the distribution of sources of the marked particles. In a turbulent fluid u_i, and hence c, are random functions which are customarily decomposed into mean ($\langle u_i\rangle$ and $\langle c\rangle$) and fluctuating (u_i' and c') components. It is then found from (1) that $\langle c\rangle$ is governed by the equation

$$\frac{\partial\langle c\rangle}{\partial t}+\frac{\partial}{\partial x_i}\langle u_i\rangle\langle c\rangle+\frac{\partial}{\partial x_i}\langle u_i'c'\rangle=S, \tag{2}$$

which is unsolvable due to the presence of the additional unknown quantity $\langle u_i'c'\rangle$. This problem, known as the closure problem, is a fundamental obstacle which impedes the progress of all Eulerian-type approaches to the analytical study of turbulent diffusion. One of the oldest and best known attempts to circumvent the closure problem is the so-called gradient transport hypothesis which dates back to Boussinesq in the nineteenth century. In the context of (2), this hypothesis states that

$$\langle u_i'c'\rangle=-K_{ij}\frac{\partial\langle c\rangle}{\partial x_j}, \tag{3}$$

where K_{ij} is a turbulent diffusivity tensor which must be evaluated using empirical data. The limitations of (3) in representing turbulent transport are well known (Corrsin, 1974). In recent years a number of more advanced closure schemes have been developed, primarily for the turbulent momentum and energy equations (see, for example, Hanjalic and Launder, 1972; Lumley and Khajeh-Nouri, 1974); but none has yet been demonstrated to be widely applicable to problems of atmospheric diffusion.

By contrast, the Lagrangian approach, starting from basic principles, leads directly to the closed equation (see, for example, Batchelor, 1949):

$$\langle c(\mathbf{x},t)\rangle=\int\int_0^t p(\mathbf{x},t\,|\,\mathbf{x}',t')S(\mathbf{x}',t')dt'd\mathbf{x}', \tag{4}$$

where $p(\mathbf{x},t|\mathbf{x}',t')$ is the conditional probability density that a marked particle released at $(\mathbf{x}',t')$ will be found

[1] Affiliated jointly with Systems Applications, Inc., San Rafael, Calif. 94903.

at $(\mathbf{x},t)$. In principle, p is a measurable Lagrangian property of the turbulence velocity field and the molecular diffusivity of the marked particles, but in practice the exact form of p is virtually unattainable due to the extreme difficulty of tracking individual particles in turbulent fluid, especially the atmosphere. Consequently, just as the closure problem impairs the utility of (2), the lack of information regarding the exact form of p hampers the use of its Lagrangian counterpart, Eq. (4). And just as various schemes have been advanced for rendering (2) solvable, various hypotheses have been proposed for implementing (4). Chief among these is the assumption that p is Gaussian. With this approximation and the assumptions that the turbulence is isotropic and stationary, it can be shown that the widely used Gaussian plume and puff models are derivable from (4). Similarly, under the hypothesis that p describes a Markov process, as would be true in a study of pure molecular diffusion, it can be shown that (4) reduces to the diffusion equation, represented by (2) and (3) (see, for example, Monin and Yaglom, 1971). (It may be noted that the Gaussian assumption for p is equivalent to a spatially constant but temporally varying eddy diffusivity.) Unfortunately, none of these models in their current forms provides a wholly adequate description of atmospheric diffusion.

Recognizing the difficulties in obtaining actual field data to test and implement turbulence theories, a number of investigators have pursued the problem of simulating turbulent flows computationally (Deardorff, 1970, 1972; Orszag and Pao, 1974). In particular, Deardorff has developed a model which simulates the turbulent planetary boundary layer, under various stability conditions, below an inversion base of constant height (Deardorff, 1970). This model opens up new avenues, through (4), to applied studies of atmospheric diffusion; because in the atmosphere where molecular diffusion has negligible effect on the distribution of mean concentration $\langle c\rangle$, the probability density p which enters in (4) may be regarded as a function solely of the turbulence velocity field and may accordingly be calculated from the numerically simulated turbulence fields. The purpose of this report is to describe some preliminary work along these lines using the turbulence model of Deardorff described above.

The main objective of this study is to use the mean concentration profiles computed from the numerically derived values of p [referred to as the numerico-empirical (NE) profiles] to assess the adequacy of conventional atmospheric diffusion theories. First, the atmospheric diffusion equation [(2) with (3)] is assessed by determining the profile of vertical eddy diffusivity that produces the closest fit of the predicted mean concentrations with the NE profiles. Second, comparisons are made between the NE profiles and those predicted by (i) the Gaussian plume formula with Pasquill-Gifford dispersion parameters, and (ii) the Gaussian puff equation with McElroy-Pooler travel-time-dependent dispersion parameters. Additional studies of the plume and puff models are also performed.

Some work related to that which we shall describe has been reported previously. Peskin (1974) considered the numerical simulation of Lagrangian turbulence motion in both two- and three-dimensional turbulent flows. Lagrangian particles were tracked to obtain information on Lagrangian autocorrelation, mean-square displacement, relative two-point displacement, and the effects of shear flow on diffusion. Riley and Patterson (1974) have also investigated Lagrangian statistics on a numerically integrated isotropic turbulent field.

2. Description of the numerical experiments

We consider the three-dimensional dispersion of marked particles in an atmospheric flow between the ground ($\hat{z}=0$) and an elevated boundary of constant height $\hat{h}$ as simulated by the planetary boundary layer model of Deardorff (1970). (In this paper the caret is used to distinguish dimensional variables from those which have been nondimensionalized.) In each of two experiments representing neutral ($\hat{h}/L=0$) and slightly unstable ($\hat{h}/L=-4.5$) atmospheric conditions, where L is the Monin-Obukhov length, 800 particles were released from points on a horizontal plane and followed for a given period of time. To simulate no-flux boundary conditions, at each time step particles which had passed below the surface level $\hat{z}=0$ or above the inversion base $\hat{z}=\hat{z}_i$ were placed back in the fluid at their image locations. Using the computed particle trajectories, we calculated the two-dimensional density function $p(\hat{x},\hat{z},t\,|\,\hat{x}',\hat{z}',t')$ in the following manner. (The components of $\mathbf{x}$ and $\mathbf{x}'$ are now taken as $\hat{x}$, $\hat{z}$ and $\hat{x}'$, $\hat{z}'$, respectively.)

First the coordinate system of each particle was transformed to a moving frame

$$\left.\begin{aligned}\xi_i(\tau)&=\hat{x}_i(\tau)-[\hat{x}_i'+\bar{u}(\hat{z}_s)\tau]\\ \zeta_i(\tau)&=\hat{z}_i(\tau)-\hat{z}_s\end{aligned}\right\},\tag{5}$$

for $i=1, 2, \ldots, 800$, where $\bar{u}(\hat{z}_s)$ is the mean value of the $\hat{x}$ component of the wind at the level of release of the particles, and $\tau=t-t'$. The function $c_i(\xi,\zeta,\tau)$ is now defined such that

$$c_i(\xi,\zeta,\tau)=\begin{cases}(\Delta\xi\Delta\zeta)^{-1}, & \text{if } \xi-\tfrac{1}{2}\Delta\xi<\xi_i(\tau)\leqslant\xi+\tfrac{1}{2}\Delta\xi\\ & \text{and } \zeta-\tfrac{1}{2}\Delta\zeta<\zeta_i(\tau)\leqslant\zeta+\tfrac{1}{2}\Delta\zeta\\ 0, & \text{otherwise.}\end{cases}\tag{5'}$$

If each single particle release is taken to constitute a separate realization, then c_i is just the concentration at (ξ,ζ,τ) in the ith realization. We now estimate the probability density $p=p(\xi,\zeta,\tau\,|\,0,0,0)$ by

$$p\approx\tilde{p}=\frac{1}{N}\sum_{i=1}^{N}c_i(\xi,\zeta,\tau),\tag{6}$$

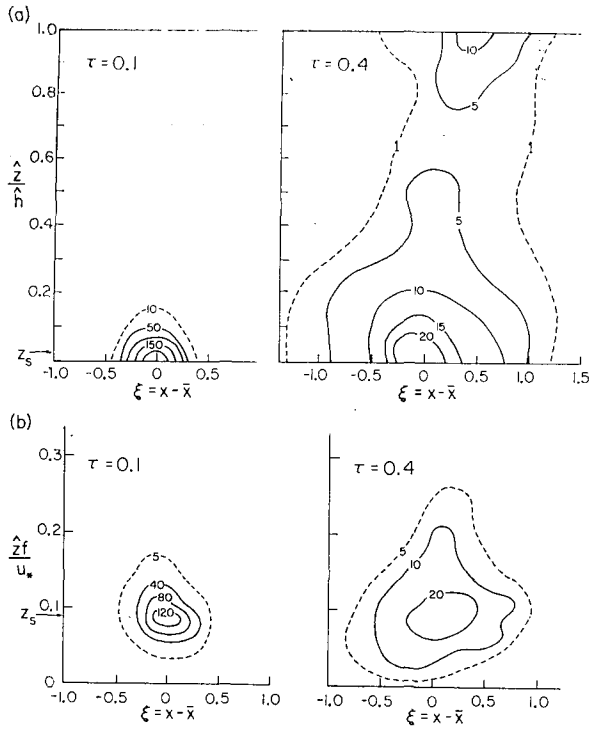

FIG. 1. The probability density function $p(\xi,z,\tau|z_s)$ (relative units) at travel time τ in a coordinate system centered at $\bar{x}=\bar{u}(z_s)\tau$, where z_s is the particle release height: (a) unstable stratification, (b) neutral case.

where $N=800$. As long as $\Delta\xi$ and $\Delta\zeta$ are small compared to the spatial scales of $\langle c\rangle$, Eq. (6) provides an unbiased estimate of p. This can be seen by taking the expectation (denoted by angle brackets) of (6) and comparing the result with (4) for the case of a unit, instantaneous point source. We have

$$\langle\tilde{p}\rangle=\frac{1}{N}\sum_{i=1}^{N}\langle c_i\rangle=\langle c\rangle=p(\xi,\eta,\tau). \tag{6'}$$

To estimate the error in (6) precisely would require a much larger data set than that available in the present study. Consequently, we shall attempt to estimate error bounds using conventional methods. Let χ represent the mean square error in the estimate $\tilde{p}$ of p, that is

$$\chi=\langle(\tilde{p}-\langle\tilde{p}\rangle)^2\rangle.$$

Using (6) and (6′) in this expression we obtain

$$\chi=\frac{1}{N^2}\sum_{i=1}^{N}\sum_{j=1}^{N}\langle c_ic_j\rangle-\langle c\rangle^2.$$

Due to the proximity of the particles to one another at their time of release, each realization c_i is correlated initially with some of the other realizations, but this correlation decays with travel time. Suppose that for each i, c_i is perfectly correlated with m other realizations, i.e., $\langle c_ic_j\rangle=\langle c^2\rangle$ for m values of j, but that it is statistically independent of all the rest. In this case we have

$$\chi=\frac{m+1}{N}(\langle c^2\rangle-\langle c\rangle^2).$$

The mean fractional error is therefore

$$\epsilon=\frac{\chi^{\frac{1}{2}}}{\langle\tilde{p}\rangle}=\frac{(m+1)^{\frac{1}{2}}(\gamma-1)^{\frac{1}{2}}}{N^{\frac{1}{2}}}, \tag{6''}$$

where $\gamma=\langle c^2\rangle/\langle c\rangle^2$.

Based on spatial correlation calculations reported by Deardorff and Peskin (1970), we estimate that for the neutral case to be analyzed in the present study, m initially has a value of about 10 and decays to zero within a travel time τ of about 0.4 (nondimensional units to be defined shortly). Comparable, or smaller, values should also pertain to the unstable case.

In view of the definition of c_i, the appropriate value of γ for use here is that which one would observe in a "plume" consisting of a single particle in turbulent fluid. Such data are not available; but if we assume that on each realization the particle is equally likely to be anywhere within a box of area $n\Delta\xi\Delta\zeta$ centered at $x=\bar{u}(z_s)\tau$, $z=z_s$, then it can be shown that $\gamma=n$.

With this and the above results we conclude that

$$\epsilon\approx\begin{cases}0.1n^{\frac{1}{2}}, & \tau\ll 0.4\\ 0.03n^{\frac{1}{2}}, & \tau\geqslant 0.4\end{cases} \tag{7}$$

To aid both in estimating ϵ and in acquiring a physical feel for the probability density p, we have plotted $\tilde{p}(\xi,z,\tau|z_s)$ in Fig. 1 for two travel times τ and for each of the two stability conditions treated. Here $\xi=x-\bar{u}(z_s)\tau$ and z_s is the particle release height. The nondimensional space and time coordinates used are defined by

$$x=\frac{\hat{x}}{\hat{h}},\quad z=\frac{\hat{z}}{\hat{h}},\quad t=\frac{\hat{t}u_*}{\hat{h}}, \tag{7'}$$

where u_* is the friction velocity and $\hat{h}$ a vertical length scale, to be defined later. In this and in all subsequent calculations, $\Delta\xi=0.2$ and $\Delta\zeta=0.05$. Using these values and Fig. 1, we may estimate the value of n required in the error formula (7). For $\tau=0.1$ we conclude that for both the neutral and unstable cases shown, $\epsilon\approx 0.2$. Similarly, for $\tau=0.5$ we estimate that $\epsilon\approx 0.5$ in the unstable case and about 0.3 in neutral conditions.

These relatively large error values are not as serious as one might suspect because our main interest here is not with the probability density itself but rather with the mean concentration distribution in a point source plume. Specifically, we shall use $\tilde{p}$ in (4) to compute the mean, steady-state crosswind-integrated concentration $\langle c(x,z)\rangle$ of a chemically inert substance issuing from a continuous point source. For this case, and with

the assumption $\langle c(x,z,t_0)\rangle=0$, we obtain from (4)

$$\langle c(x,z)\rangle=\lim_{t\to\infty} M\int_0^t p(x,z,t\,|\,x_s,z_s,t')dt', \tag{8}$$

where M and (x_s,z_s) denote the emission rate and location, respectively, of the point source. The time integration in (8) effectively reduces the dimensionality of the probability density estimate $\tilde{p}$. To account for this, and for a small-scale space averaging operation that is used to smooth $\langle c(x,z)\rangle$, the following value of n should be used in the error formula (7):

$$n=\max\{1, \min\{20\sigma_z, 10\}\}.$$

The resulting error in the concentration field is found to be about 10%, in both the neutral and unstable cases, over the entire length of the plume and within the core region out to a distance of about $2\sigma_z$ from the plume centerline. Results of the $\langle c(x,z)\rangle$ calculations will be presented later.

3. Assessment of the atmospheric diffusion equation

It was mentioned in the Introduction that the implications of the gradient transport hypothesis (3) regarding the nature of turbulent diffusion has inherent limitations. However, the so-called diffusion equation to which this hypothesis gives rise through (2) is a very attractive equation from the standpoint of describing atmospheric diffusion. This is because this equation is simple; it is easily solvable using conventional finite-differencing techniques; and it lumps the effects of the turbulence into the single function K_{ij} rather than in one or several additional differential equations. The latter property is particularly useful in modeling chemically reacting air pollutants because in that case the number of differential equations involved for the mean concentrations alone is often quite large. These considerations therefore prompt the question: Does a function K_{ij} exist which renders the differences between the solution of the diffusion equation and the NE solution of (4) acceptably small, and if so, how does this "optimal" diffusivity compare with the expressions in current use? As an added constraint, we insist that the function K_{ij} depend on spatial coordinates only and not on travel time. Without this restriction, which is contradictory to observations, K_{ij} would become a function of the source distribution S and would therefore acquire extremely unwieldly forms in problems such as urban pollution modeling where there exists a multitude of widely scattered sources of various shapes and sizes and temporally variable strengths. In short, we are attempting to determine whether turbulent diffusion can be described with acceptable accuracy in terms of some local, hypothetical property of the flow field.

To explore this question we consider the two-dimensional steady-state form of the atmospheric diffusion equation in which turbulent dispersion in the direction of the mean wind is neglected, i.e.,

$$\bar{u}(\hat{z})\frac{\partial\langle c\rangle}{\partial\hat{x}}=\frac{\partial}{\partial\hat{z}}\left(\hat{K}_Z(\hat{z})\frac{\partial\langle c\rangle}{\partial\hat{z}}\right)+M\hat{\delta}(\hat{x}-\hat{x}_s)\delta(\hat{z}-\hat{z}_s). \tag{9}$$

Upon defining the dimensionless variables,

$$u=\frac{\bar{u}}{u_*},\quad K_Z=\frac{\hat{K}_Z}{u_*\hat{h}},\quad C=\frac{\langle c\rangle\bar{u}(\hat{z}_s)\hat{h}}{M},$$

where $\hat{h}$ is a vertical length scale and u_* the friction velocity, we obtain the dimensionless form of (9)

$$u\frac{\partial C}{\partial x}=\frac{\partial}{\partial z}\left(K_Z\frac{\partial C}{\partial z}\right)+\left(\frac{\bar{u}(\hat{z}_s)}{u_*}\right)\delta(x-x_s)\delta(z-z_s), \tag{10}$$

where $\delta(\cdot)=\hat{\delta}(\cdot)\hat{h}$ and where x, z and t are given by (7′). The boundary conditions for (10) are

$$C(0,z)=0, \tag{11}$$

$$K_Z\frac{\partial C}{\partial z}=0,\quad z=0, 1. \tag{12}$$

In contrast to the neutral case where the depth of the planetary boundary layer is some fraction of u_*/f, where f is the Coriolis parameter, Deardorff found that the unstable boundary layer extends up to the height z_i of the inversion base below which convective mixing is confined. Consequently, the proper choice of the length scale $\hat{h}$ is $\hat{h}=z_i$ in unstable cases and $\hat{h}=u_*/f$ in the neutral case.

Before proceeding to the calculation of the optimal diffusivity K_Z, we consider first the mean velocity profiles u that enter into (10) and also the diffusivity profiles K_Z in current use.

a. Wind profiles from the planetary boundary layer model

Fig. 2 shows $u(z)$ computed by the planetary boundary layer model in the two cases of $\hat{h}/L=0$ and -4.5. It is of interest to compare these profiles with those predicted by conventional theories.

In Monin-Obukhov similarity theory, the mean velocity gradient in the surface layer is given by (Monin and Yaglom, 1971)

$$\frac{\partial\bar{u}}{\partial\hat{z}}=\frac{u_*}{\kappa\hat{z}}\hat{\phi}_m\left(\frac{\hat{z}}{L}\right), \tag{13}$$

where

$$\hat{\phi}_m\left(\frac{\hat{z}}{L}\right)=\begin{cases}1, & \hat{z}<\kappa u_*/f\ [\text{neutral}]\\ \left(1-\beta\dfrac{\hat{z}}{L}\right)^{-0.25}, & -2<\hat{z}/L<0\ [\text{unstable}]\end{cases} \tag{14}$$

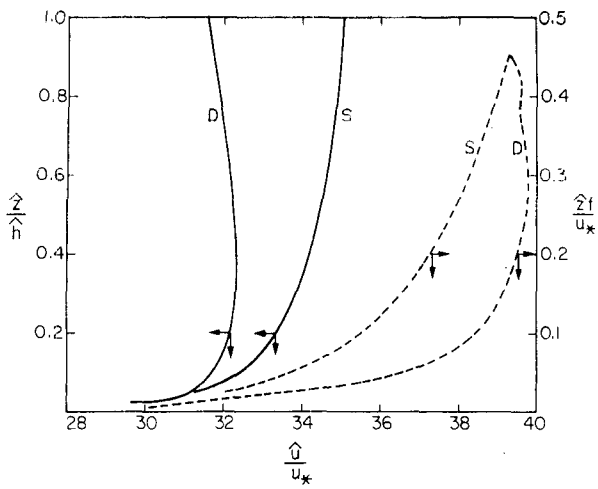

FIG. 2. Wind profiles given by similarity theory (S) and Deardorff's model (D) for neutral (dashed curves) and unstable ($\hat{h}/L=-4.5$) conditions.

The commonly accepted value of β is 15 and the von Kármán constant κ is approximately 0.35.

The mean surface layer velocity profiles obtained by integrating (13) from $\hat{z}_0$ to $\hat{z}+\hat{z}_0$ are given in Table 1, where the profiles are expressed in both dimensional and dimensionless form.

Above the surface layer there is a change of wind direction with height (the Ekman layer). In the planetary boundary layer it is found that $\bar{v}\approx\frac{1}{5}\bar{u}$ at the geostrophic level, so that $|\mathbf{v}|\approx\bar{u}$, even with turning. In the unstable case, i.e. $\hat{z}_i/L\lesssim-1.5$, both observational data and the numerical calculation show that change of wind direction is strongly suppressed, resulting in a nearly unidirectional flow in the planetary boundary layer. In the diffusion calculations to be presented later, the turning of the wind with height is neglected in all situations.

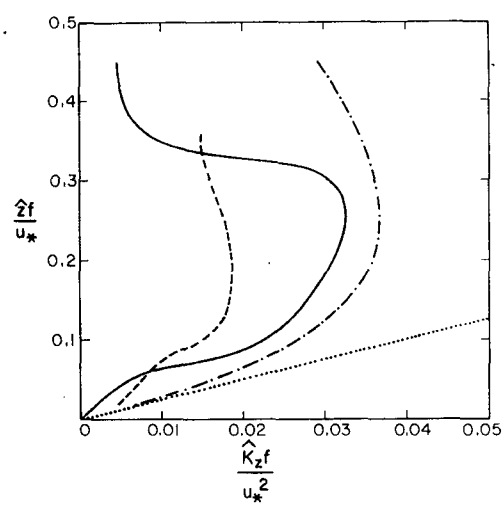

FIG. 3. Comparison of the optimal K_Z profile (solid curve) with the profile proposed by Shir and Shieh (dash-dotted); the profile given by similarity theory (dotted); and the eddy viscosity calculated by Deardorff (dashed) in the neutral ($\hat{h}/L=0$) boundary layer.

TABLE 1. Wind and vertical eddy diffusivity profiles in the surface layer from similarity theory.

	Neutral ($\hat{z}<\kappa u_*/f$)	Unstable ($-2<z/L<0$)
$\bar{u}(\hat{z})$	$\frac{u_*}{\kappa}\ln\left(1+\frac{\hat{z}}{\hat{z}_0}\right)$	$\frac{u_*}{\kappa}\left[2(\tan^{-1}\hat{\psi}-\tan^{-1}\hat{\psi}_0)+\ln\left(\frac{\hat{\psi}+1}{\hat{\psi}_0-1}\right)-\ln\left(\frac{\hat{\psi}+1}{\hat{\psi}_0+1}\right)\right]$
$u(z)$	$\frac{1}{\kappa}\ln\left(1+\frac{z}{z_0}\right)$	$\frac{1}{\kappa}\left[2(\tan^{-1}\psi-\tan^{-1}\psi_0)+\ln\left(\frac{\psi-1}{\psi_0-1}\right)-\ln\left(\frac{\psi+1}{\psi_0+1}\right)\right]$
$\hat{K}_Z(\hat{z})$	$\kappa u_*\hat{z}$	$\kappa u_*\hat{z}\left(1-\beta\frac{\hat{z}}{L}\right)^{-0.25}$
$K_Z(z)$	κz	$\kappa z\left(1-\beta z\frac{\hat{h}}{L}\right)^{-0.25}$

Note: $\hat{\psi}=[1-\beta(\hat{z}+\hat{z}_0)/L]^{\frac{1}{4}}$, $\hat{\psi}_0=(1-\beta\hat{z}_0/L)^{\frac{1}{4}}$.
$\psi=[1-\beta(z+z_0)\hat{h}/L]^{\frac{1}{4}}$, $\psi_0=(1-\beta z_0\hat{h}/L)^{\frac{1}{4}}$.

Although several approximate expressions have been proposed to describe the wind speed profile above the surface layer, none of these agrees as well with the numerically calculated wind as the profile obtained by simply extrapolating the surface layer formulation [Eqs. (13)–(14)] to the top of the boundary layer. A comparison of these profiles is presented in Fig. 2.

b. *Theoretical forms for eddy diffusivities*

The surface layer vertical eddy diffusivities corresponding to the mean wind profiles derived from similarity theory are given in Table 1 and shown in Figs. 3 and 4. Considerably less is known about the behavior of K_Z above the surface layer than within it. In two recent studies, expressions for K_Z in the planetary boundary layer above the surface layer have been proposed.

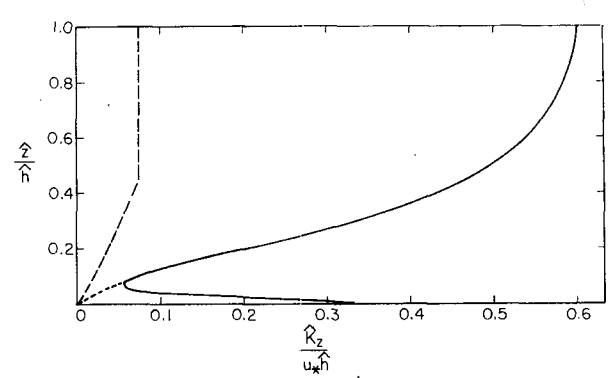

FIG. 4. Comparison of the optimal K_Z profile (solid curve) with the profile, based on similarity theory, proposed by Ragland (dashed), in the unstable ($\hat{h}/L=-4.5$) boundary layer. (See text for explanation of short dashed line.)

Ragland (1973) has suggested that $\hat{K}_Z$ be taken as constant above the surface layer at its value at the top of the surface layer. Shir and Shieh (1974), on the other hand, have assumed that $\hat{K}_Z$ obeys the following form in the planetary boundary layer:

Under neutral conditions

$$\hat{K}_Z = u_* l(\hat{z}), \tag{15}$$

where $l(\hat{z}) = \kappa\hat{z}\exp(-4\hat{z}/z_i)$.

Under non-neutral conditions

$$\hat{K}_Z(\hat{z}) = \hat{K}_Z(\hat{z}_1)\frac{l(\hat{z})}{l(\hat{z}_1)}, \tag{16}$$

where $\hat{z}_1$ is taken as 10 m; $\hat{K}_Z(\hat{z}_1)$ is to be calculated assuming $\hat{z}_1 = 10$ m lies within the surface layer.

In the dimensionless form adopted here, (15) and (16) become respectively

$$K_Z = \kappa z e^{-4z}, \tag{17}$$

$$K_Z(z) = K_Z(z_1)\left[\frac{z}{z_1}e^{4(z_1-z)}\right]. \tag{18}$$

For the region above the surface layer, K_Z profiles have been computed based on Ragland's suggestion and based on the expressions of Shir and Shieh. With the exception of (18), which constitutes a family of curves in the non-dimensionalized coordinate system, the above profiles are shown in Figs. 3 and 4.

c. *Estimation of the optimal $K_Z(z)$ in the atmospheric diffusion equation*

In addressing the question of the existence of an optimal diffusivity K_Z, one faces the general problem of estimating the form of a functional parameter appearing in a partial differential equation, namely (10), such that the solution of that equation matches certain given data as closely as possible. If the data are available as continuous functions of x and z, denoted here by $C_l(x,z)$, then the customary criterion to be minimized by choice of $K_Z(z)$ is

$$J = \int_0^{l_0}\int_0^1 [C_l(x,z) - C(x,z)]^2 dz dx, \tag{19}$$

where l_0 is the extent of x over which data are available.

This problem is known in mathematics as an *inverse problem*. It has been shown by Chen and Seinfeld (1972) that problems of the type encountered here can be solved efficiently by techniques of optimal control theory. The method which we now describe has been tested on a number of sample and actual problems (see, for example, Chen *et al.*, 1974). In this paper we will only describe the essential features of the method as required for the current problem. The reader may consult Lions (1971) or either of the references just cited for further details on optimal control theory for partial differential equations.

The optimal control problem to be solved is the following: Determine the function $K_Z(z)$ which minimizes J subject to (10)–(12) and $K_Z \geqslant 0$. Necessary conditions for optimality can be derived for this problem, conditions which assume the form of a two-point boundary value problem. These conditions are

$$u\frac{\partial C}{\partial x} = \frac{\partial}{\partial z}\left(K_Z\frac{\partial C}{\partial z}\right) + \left(\frac{\hat{u}}{u_*}\right)\delta(x-x_s)\delta(z-z_s), \tag{20}$$

$$C(0,z) = 0, \tag{21}$$

$$K_Z\frac{\partial C}{\partial z} = 0, \quad z = 0, 1, \tag{22}$$

$$\frac{\partial\psi}{\partial x} = -\frac{\partial}{\partial z}\left[K_Z\frac{\partial}{\partial z}\left(\frac{\psi}{u}\right)\right] + 2[C_l(x,z) - C(x,z)], \tag{23}$$

$$\psi(l_0,z) = 0, \tag{24}$$

$$K_Z\frac{\partial}{\partial z}\left(\frac{\psi}{u}\right) = 0, \quad z = 0, 1, \tag{25}$$

$$\frac{\delta J}{\delta K_Z} = -\int_0^{l_0}\frac{\partial C}{\partial z}\frac{\partial}{\partial z}\left(\frac{\psi}{u}\right)dx = 0, \tag{26}$$

where $\delta J/\delta K_Z$ is the functional derivative of J with respect to K_Z and $\psi(x,z)$ is the adjoint variable to $C(x,z)$ as shown, for example, by Lions (1971).

The two-point boundary value problem given by (20)–(26) cannot be solved analytically, and therefore must be solved iteratively. A straightforward means of determining the optimal value of K_Z numerically is by the method of steepest descent. From the definition of the functional derivative we can rewrite (26) as

$$\delta J = -\int_0^1\left\{\int_0^{l_0}\left[\frac{\partial}{\partial z}\left(\frac{\psi}{u}\right)\right]\left(\frac{\partial C}{\partial z}\right)dx\right\}\delta K_Z(z)dz, \tag{27}$$

which is a direct expression for the effect of a perturbation in K_Z on the value of J. The basis of the method of steepest descent is to choose δK_Z such that δJ is negative. This is accomplished by setting

$$\delta K_Z(z) = W(z)\int_0^{l_0}\left[\frac{\partial}{\partial x}\left(\frac{\psi}{u}\right)\right]\left(\frac{\partial C}{\partial z}\right)dx, \tag{28}$$

where $W(z)$ is an arbitrary, positive function of z.

The algorithm proceeds as follows:

1) Make an initial guess of $K_Z(z)$; call it $K_Z^0(z)$. Select $W(z)$.

2) Integrate (20)–(22) from $x=0$ to $x=l_0$ using K_Z^0. Evaluate J.

3) Integrate (23)–(25) from $x=l_0$ to $x=0$ using K_Z^0 and $C(x,z)$ from step 2.

4) Compute δK_Z from (28); call it δK_Z^0.

5) Revise the initial guess of K_Z by $K_Z^1 = K_Z^0 + \delta K_Z^0$. If $K_Z^1 < 0$, set $K_Z = 0$.

6) Using K_Z^1, return to step 2 and repeat.

7) Continue until $(J^n - J^{n+1})/J^n < \epsilon$, where ϵ is a preset convergence criterion.

In the steepest descent algorithm, the perturbations in K_Z are defined in order to seek the minimum of J by moving K_Z along the gradient of J with respect to K_Z. The length of the step, i.e., how far a distance one proceeds along the gradient in each direction, is controlled by the choice of the function $W(z)$. Although it is possible to choose $W(z)$ by an auxiliary optimization problem, it is generally simpler computationally to select a constant value of W initially equal, say, to some fraction of the initial guess of K_Z. If, during the iteration, an improved estimate of K_Z increases rather than decreases J, the minimum has been overstepped. We then go back to the value from the previous iteration and decrease W by a preset factor before computing the new estimate. The convergent value of K_Z will generally vary depending on the initial guess. Thus, it is necessary to try several different initial guesses to determine the variability of the convergent K_Z profiles. This procedure was carried out in the present study, and the profiles to be discussed subsequently were substantially attained regardless of the initial guess. Nevertheless, results on the uniqueness of profiles determined by optimal control theory are still unavailable.

The resulting optimal diffusivity profile $K_Z(z)$ for the neutral case is shown in Fig. 3 and for the unstable case in Fig. 4. There is relatively good agreement between the neutral profile and that proposed by Shir and Shieh. There is also fairly close correspondence to the eddy viscosity profile computed by Deardorff. Although we show in Fig. 3 the eddy viscosity profile computed by Deardorff, there is no reason to expect that the eddy diffusivity for mass and the eddy viscosity for momentum should coincide. We would expect the two parameters to have a similar dependence on height, however, as was found in this study. The diffusivity estimates given by similarity theory are everywhere too large and differ from the optimal value by nearly a factor of 10 at the top of the boundary layer.

The opposite situation is found in the unstable case (Fig. 4) where the optimal diffusivities are much larger than those given by similarity theory. When the latter values were used in (10), the resulting errors were a factor of 10 larger than those produced by the optimal K_Z profile. For all common values of $\hat{h}$, the Shir-Shieh profile for K_Z in unstable conditions (not shown in Fig. 4) gives smaller diffusivities than similarity theory.

The fact that the optimal K_Z profile does not drop to zero along the broken line shown in Fig. 4 cannot be attributed to the algorithm that was used to compute

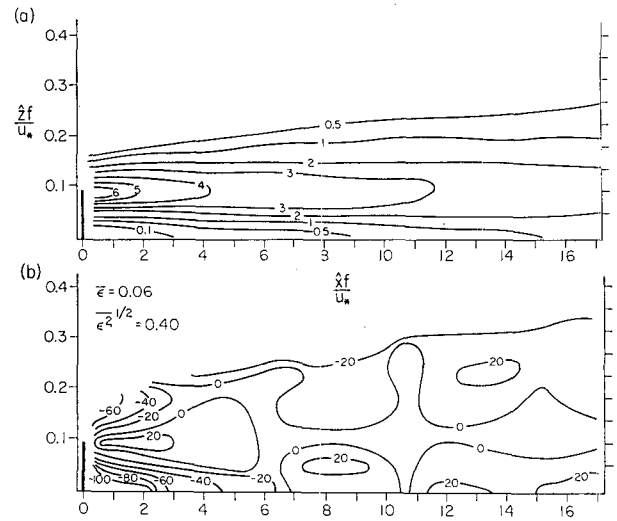

FIG. 5. (a) Nondimensionalized crosswind-integrated concentrations computed from Eq. (4) using the probability density p calculated from Deardorff's data for neutral ($\hat{h}/L=0$) stability. (b) Concentrations given by the diffusion equation (10) using the optimum K_Z profile shown in Fig. 3 and the wind profile (D) in Fig. 2. Concentrations are expressed as the percentage deviation (i.e., 100ϵ) from those given in 5a.

K_Z, because it was found that the smaller diffusivity values near the surface resulted in larger errors in the ground-level concentrations predicted by (10). A more likely cause is the larger truncation errors in the finite-difference model of (10).

Having described the differences between the optimal K_Z profile and some of the diffusivity formulas in current use, we turn now to the important question of how well the solutions of (10), using the optimal profiles, compare with the corresponding NE solutions of (4). The latter are displayed in Figs. 5a and 6a for the neutral and unstable cases, respectively. Note that

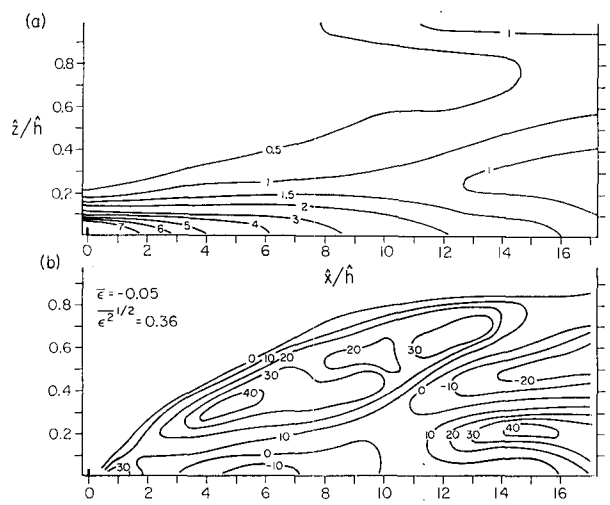

FIG. 6. As in Fig. 5 except for the unstable ($\hat{h}/L=-4.5$) case.

in the neutral case the source height $z_s=0.2$ and in the unstable case, $z_s=0.025$. To facilitate a comparison of these solutions with those of (10), we have plotted the latter in Figs. 5b and 6b in the form a fractional error

$$\epsilon(x,z)=\frac{C(x,z)-C_0(x,z)}{C_0(x,z)}, \tag{29}$$

where C denotes the solution of (10) and C_0 represents the corresponding value given by (4). The figures give the values of ϵ multiplied by 100 so we may interpret them as plots of the percentage error.

The figures reveal that the errors in (10) are nearly randomly distributed in space except for the neutral case where rather large errors occur near the source. That the errors are larger in this region is consistent with the conclusion drawn from theoretical considerations that the gradient transport hypothesis should not hold when the length scale of the mean concentration distribution is comparable to or smaller than the Lagrangian length scale of the turbulence. For the most part, however, it appears that this hypothesis is reasonable. Errors in the calculated concentrations are no larger than about 20% at points farther than about $6\,u_*/f$ from the source in the neutral case and at nearly all points at ground level in the unstable case. The large values of ϵ in regions away from the large values of C_0 could, of course, be due to statistical scatter of the data, since ϵ, as defined, enhances statistical scatter in regions of small C_0.

In summary, we have introduced a technique by which diffusivity profiles (or, in a simpler case, parameters in a profile expression of an assumed form) can be determined from field or numerical turbulent diffusion data. The value of the technique lies in the ability it provides of determining the diffusivity profile that best matches given data, assuming that the data are to be interpreted through the atmospheric diffusion equation. The eddy diffusivity is, of course, merely an empirical parameter which should be determined on the basis of experimental data. Such an exercise does provide some indication as to the validity of the atmospheric diffusion equation, since the discrepancy between the data and the predictions of the equation using the best value of the eddy diffusivity is a measure of the accuracy of the equation.

4. Analysis of the dispersion parameters σ_z and σ_x in the plume and puff models

As previously mentioned, both the plume and puff models assume that the probability density function p which enters in (4) has a Gaussian form that is completely determined by the mean $(\bar{x},\bar{z})$ and mean square $(\overline{x^2},\overline{z^2})$ displacements of fluid particles from their point of release. Recall that these quantities are properties of the turbulence. Because of the great difficulty of tracking particles in the atmosphere, past empirical studies of atmospheric diffusion have not attempted to measure the particle displacement statistics directly. Rather $\overline{x^2}$ and $\overline{z^2}$ have been treated merely as free parameters to be used in fitting a Gaussian profile to concentration measurements made downwind from point sources of known strength under various atmospheric conditions. It was in this manner that the so-called dispersion parameters of Pasquill-Gifford (PG) and McElroy-Pooler (MP) were obtained. If the probability density p were actually Gaussian and if the assumptions involved in the empirical determination of the dispersion parameters were correct, then these parameters should be equivalent to the mean-square particle displacements $\overline{x^2}$ and $\overline{z^2}$. Let us compare the profiles of $\overline{x^2}$ and $\overline{z^2}$ calculated from the particle trajectories given by Deardorff's model with the dispersion parameters measured in the two empirical studies just cited.

The PG data give a vertical dispersion parameter σ_z as a function of distance x from the source for various atmospheric stabilities. *In principle*, the parameter σ_z is related to the particle displacement statistics by

$$\sigma_z^2=\overline{(z-z_s)^2},$$

where z_s is the height of release of the particles. In the plume and puff models it is generally assumed that $\bar{x}$ is equivalent to distance x from the source and that $\bar{z}=z_s$.

The computed values of $\overline{(z-z_s)^2}$ vs $\bar{x}$ for both the neutral and unstable cases are shown in Fig. 7 by the open triangles and open circles, respectively. In the same figure, the nondimensionalized PG profiles of σ_z vs $\bar{x}$ for three different atmospheric stabilities are indicated by the curves. Since the positions, but not the slopes, of these curves are dependent on the value of the length scale $\hat{h}$ that is used to non-dimensionalize σ_z and $\bar{x}$, we have indicated the extent to which each curve would be displaced by a different choice of $\hat{h}$.

It is immediately clear from the figure that the calculated and measured σ's are in poor agreement. The chief discrepancy is a systematic shift of the calculated values to the right of the measured ones. Thus, if we plot $\overline{(z-z_s)^2}$ vs $0.24\bar{x}$, we get the closed circles and triangles shown in Fig. 7 and these are in much better agreement with the measurements. Note that in both the neutral and unstable cases, the slope of the computed σ_z profile conforms for small distances x to that of the PG profile for class C stability (i.e., slightly unstable); but that at greater distances, the slopes become dissimilar, the unstable case becoming parallel to the class B profile and the neutral case becoming parallel to the class D curve.

That a smaller value of $\bar{x}$, namely $0.24\bar{x}$, should bring the computed and measured data into closer agreement suggests that the PG data pertain to particles released from a lower level than that used in the numerical experiments. This follows from the fact that

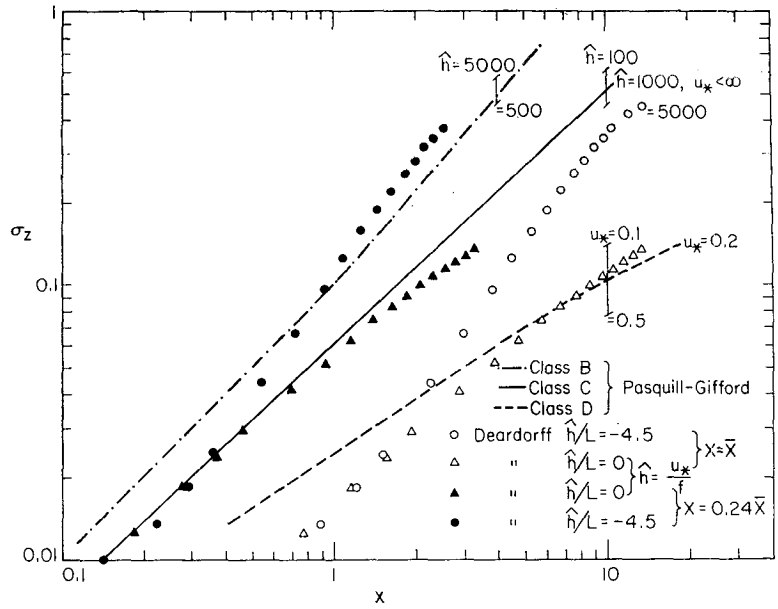

FIG. 7. Comparison of the computed nondimensionalized root-mean-square vertical particle displacement σ_z (circles and triangles) with the Pasquill-Gifford σ_z dispersion parameter (curves) for neutral and unstable conditions as a function of downwind distance x from the source.

for a release height z', $d\bar{x}/dt \approx \bar{u}(z')$; and thus with a strong wind shear near the ground (see Fig. 2) $\bar{x}$ will increase with z' for a given value of the travel time t. This effect is apparently not taken into account in routine diffusion estimates made with the plume formula (see Turner, 1969). Consequently, one could expect those calculations systematically to overestimate the ground-level concentrations resulting from elevated sources, if, as appears likely, σ_z is less sensitive to z' than $\bar{x}$ is.

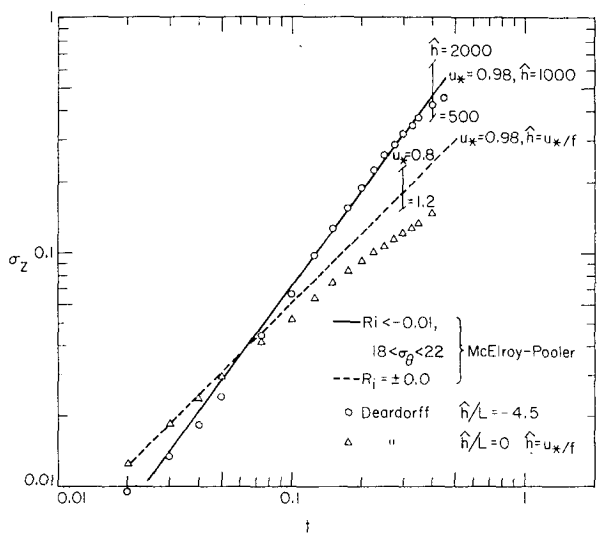

FIG. 8. As in Fig. 7 except for comparison with the McElroy-Pooler dispersion parameter as a function of travel time t.

The PG dispersion parameters are useful only in the plume formula. The puff model, however, requires σ's that are functions of travel time. Data of this type have been collected by McElroy and Pooler in St. Louis (see McElroy, 1969) and are shown in nondimensional form in Fig. 8 alongside the computed values of σ_z for the same stability cases. Again we note that the positions, but not the slopes, of the empirical curves are dependent on the values of the length scale $\hat{h}$ and the time scale $\hat{h}/u_*$ that are used to nondimensionalize the data. It is seen that for a value of $u^*=0.98$ m s^{-1}, which is not unreasonable for the urban area in which the MP data were collected, the computed and measured $\sigma_z(t)$ profiles are in excellent agreement in the unstable case and good agreement, for small t, in neutral conditions. (The downward turning of the computed σ_z profile at large t is a result of the effect of the simulated inversion base, at $z=1$, in the numerical model.)

Fig. 9 compares the computed *streamwise* dispersion $\sigma_x=(\overline{x^2}-\bar{x}^2)^{\frac{1}{2}}$ with the *lateral* dispersion $\sigma_y=(\overline{y^2}-\bar{y}^2)^{\frac{1}{2}}$ observed by MP as a function of travel time. (We did not compute σ_y originally because it is not needed in our problem.) According to Corrsin (1959) and to the results of numerical experiments performed by Deardorff and Peskin (1970), in a constant shear flow the streamwise dispersion σ_x^2 should increase as t^3 at large travel times t while the lateral dispersion σ_y^2 should grow as t. We cannot expect these results to apply here, however, because in the present study only the initial portion of the flight of each particle is spent in the shear layer near the ground. This can be seen by comparing

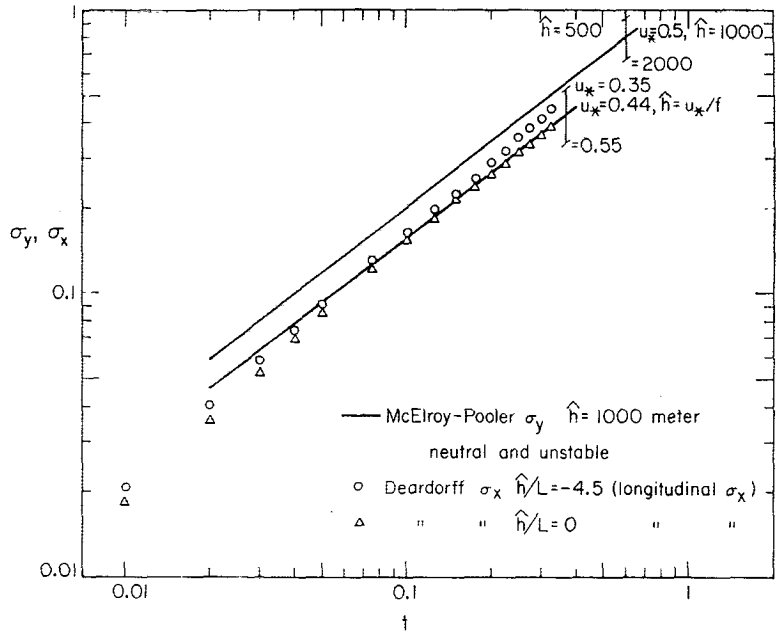

FIG. 9. Comparison of the computed nondimensionalized streamwise root-mean-square particle displacement σ_x (circles and triangles) with the McElroy-Pooler lateral dispersion parameter σ_y for neutral and unstable conditions as a function of travel time t.

the wind profiles of Fig. 2 with the particle release heights: $\hat{z}_s=0.025\ \hat{z}_i$, unstable; $\hat{z}_s=0.09\ u_*/f$, neutral. As travel time increases, many of the particles are carried up into the region above the surface layer where there is little or no shear. The rate at which this process occurs can be estimated from the probability density function shown in Fig. 1.

The MP data for σ_y show little variation between neutral and unstable conditions. The same behavior is exhibited by the computed σ_x values. In fact, it is shown in Fig. 9 that when the empirical data are non-dimensionalized using a friction velocity of about 0.45 m s^{-1}, about one-half the value used earlier with σ_z, the computed and observed dispersion curves are nearly superposed.

Recall that if the turbulence were such that the probability density p which enters in the generalized diffusion equation (4) (and in the puff equation) were actually Gaussian with joint moments $\overline{xy}=\overline{xz}=\overline{yz}=0$ as the puff model assumes, then the empirical σ's would be equivalent to the root-mean-square second moments of p, i.e., $(\overline{x^2})^{\frac{1}{2}}$, $(\overline{z^2})^{\frac{1}{2}}$, etc., as described earlier, and the concentrations predicted by the puff model would be in exact agreement with those given by (4). It follows, therefore, that since the empirical σ's are in close agreement with the numerically calculated values of $(\overline{x^2})^{\frac{1}{2}}$, $(\overline{z^2})^{\frac{1}{2}}$, etc., major errors in the puff model predictions will reflect departures of the turbulence characteristics from those consistent with the assumed Gaussian form of p. Similar arguments apply to the plume formula. Let us examine these errors.

For this purpose we set up the standard plume model, using PG dispersion data, and the puff model of Lamb and Neiburger (1971), using the MP data, to simulate the same two-dimensional problem that was treated earlier in Section 3. In each case the empirical data were non-dimensionalized in the manner portrayed in Figs. 7, 8 and 9 so that each set was in closest agreement with the computed particle statistics $\overline{x^2}$, $\overline{z^2}$, etc. It should be pointed out that the plume model does not account rigorously for the effects of the inversion layer present in this problem. However, in the trial calculations to be presented, this deficiency is not serious, because within the range of downwind distances treated, the inversion layer has little overall influence on the concentration distributions.

The results of the calculations for the neutral case are shown in Fig. 10 and for the unstable case in Fig. 11. As in the previous section we have plotted the model predictions in terms of their fractional departure ϵ [Eq. (29)] from the corresponding NE solutions of (4). The latter are given in Figs. 5a and 6a. We shall consider only the puff model results here, because due to the better agreement between the MP data and the computed particle statistics, these results provide a better assessment of the accuracy of the assumed Gaussian form of p.

Looking first at Fig. 8, we see that for the neutral case the empirical and the calculated σ_z profiles are nearly superposed for travel times $t\lesssim 0.1$, which corresponds to distances x from the source in the range $0<x\lesssim 4$. However, Fig. 10a reveals that in this range

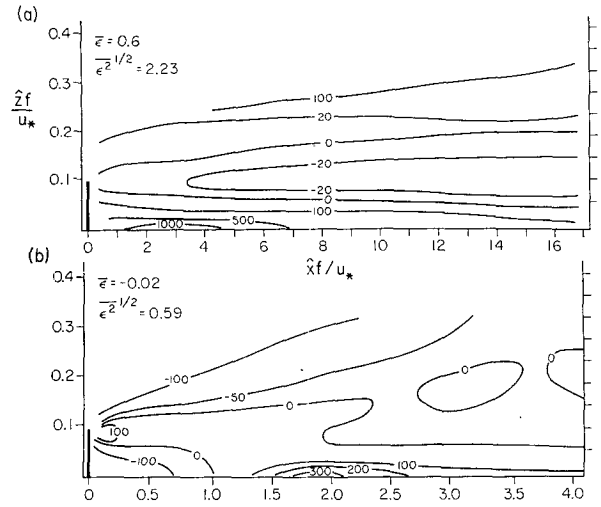

FIG. 10. (a) Nondimensionalized crosswind-integrated concentrations predicted by the puff model expressed as the percentage deviation (i.e., 100ϵ) from those shown in Fig. 5a which were obtained from Eq. (4) for the case of neutral stability. (b) Results of the plume model calculations expressed as in (a). The puff model uses neutral, travel-time dependent MP data; the plume model uses PG class C data and an expanded x axis (see text).

the predictions of the puff model are considerably in error. Concentrations are underestimated on the centerline of the plume and are greatly overestimated at the edges, especially along the plume edge that touches the ground. This behavior suggests that the diffusing particles behave as though there were a weak restoring force which tends to prevent them from wandering too far away from their level of release, i.e., the plume axis. Thus, particles that have wandered a distance σ_z, say, from the plume axis have a larger probability of moving

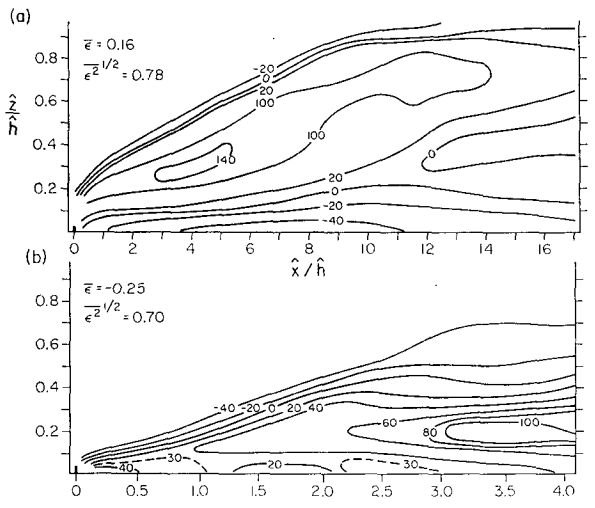

FIG. 11. As in Fig. 10 except for unstable ($\hat{h}/L = -4.5$) case with class B data used in the plume model and "slightly unstable" MP data in the puff model. The corresponding solutions of Eq. (4) are shown in Fig. 6a.

back toward the plume centerline than of continuing on to still more remote points. By contrast, the Gaussian density implies that at each instant the particles have equal probabilities of moving toward or away from the plume axis. In short, the Gaussian density has a much larger kurtosis or flatness factor than the true probability density p under neutral conditions.

Turning next to the unstable case, we see in Fig. 8 that here the measured and computed values of σ_z are in excellent agreement at all travel times (and distances from the source) except those at the extreme upper limit of the range treated. Fig. 11a reveals that the errors in the puff model predictions are smaller in this instance than in the neutral case but that there is still a tendency for the predicted concentrations along the plume centerline to be too small and those at the edges to be too large. One factor contributing to these errors is the assumption in the puff model that the joint moment $\overline{xz}$ is zero. In actuality, this moment is strongly positive because due to the rapid increase in wind speed above the level of release of the particles in the unstable case (see Fig. 2), particles which are displaced upward are also systematically displaced downstream. Consequently, at any distance x from the source, a significant fraction of the particles that normally would be found at the plume edge are now found farther downstream and in their places particles from points upstream of x, and hence with smaller vertical displacements, now reside. As a result, the effective width of the plume is everywhere smaller than one would predict based on σ_z alone. This phenomenon is not as pronounced in the neutral case because there the wind shear at the level of release of the particles is much smaller (see Fig. 2).

The analyses just completed serve to illustrate the inadequacy of the basic assumption underlying the plume and puff models, namely that the probability density p which enters in (4) is of the Gaussian form. However, despite these limitations, the plume and puff models remain attractive formulations in applied studies because of their mathematical simplicity. For this reason it is useful to inquire whether σ profiles exist which will bring the errors in the predictions of these two models within the range of acceptability.

To explore this question we used the variances $\sigma_x(\tau)$ and $\sigma_z(\tau)$ as adjustable parameters for obtaining a least-squares best fit of the Gaussian density function to the numerico-empirical expression p. The resulting "optimal" profiles of σ_x and σ_z are presented in Figs. 12 and 13, respectively. In each case the corresponding empirical data of McElroy-Pooler, presented earlier in Figs. 8 and 9, are shown for comparison. Considering the fact that the method used to obtain the empirical data is very similar to that used here to obtain the optimal σ_x and σ_z values, it is surprising that the latter do not compare as well with the empirical data as do the computed root-mean-square particle displacements shown in Figs. 8 and 9.

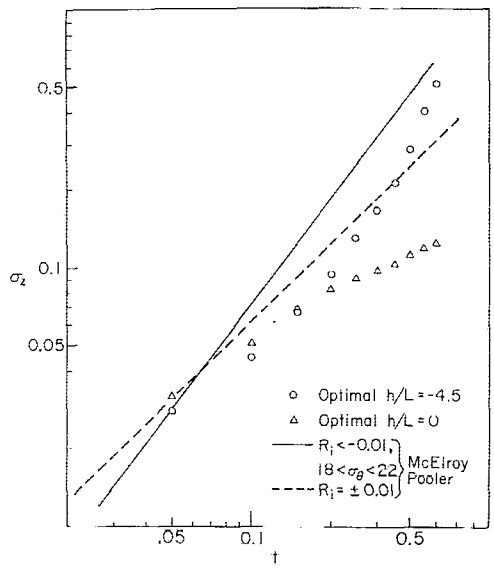

FIG. 12. Optimal $\sigma_z(t)$ profiles for use in the puff model compared with the empirical data of McElroy-Pooler.

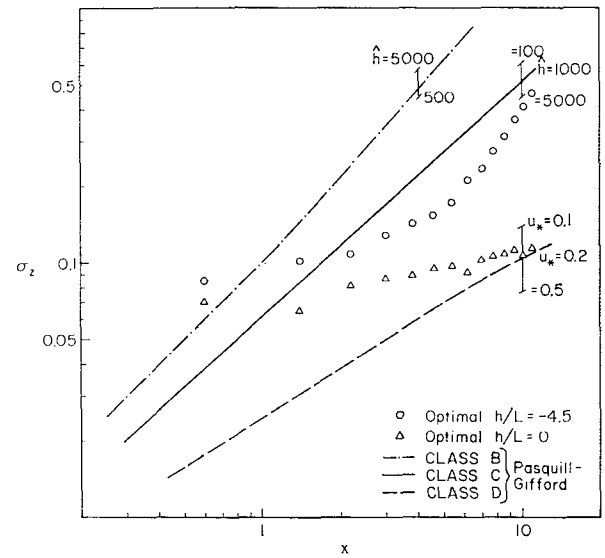

FIG. 14. Optimal $\sigma_z(x)$ profiles for use in the plume formula compared with the empirical data of Pasquill-Gifford.

In a similar manner we adjusted the dispersion parameter $\sigma_z(x)$ to obtain the least-squares best fit of the plume formula to the numerico-empirical concentration distributions given in Figs. 5a and 6a. The results are presented in Fig. 14. The empirical Pasquill-Gifford data are also shown for comparison.

These "optimal" dispersion coefficients were subsequently inserted into the puff and plume models and new sets of calculations were performed to compare with the NE concentration profiles given in Figs. 5a and 6a. The results, given in terms of the fractional error ϵ used earlier, are presented in Fig. 15 for the neutral case and in Fig. 16 for the unstable case. On comparing Figs. 10a and 11a with Figs. 15a and 16a, we find that while the overall performance of the puff model has been improved by the optimal σ_x and σ_z profiles, errors in the predicted values remain intolerably large in certain regions. This is especially true in the case of the ground-level concentrations predicted in the neutral case (See Fig. 15a).

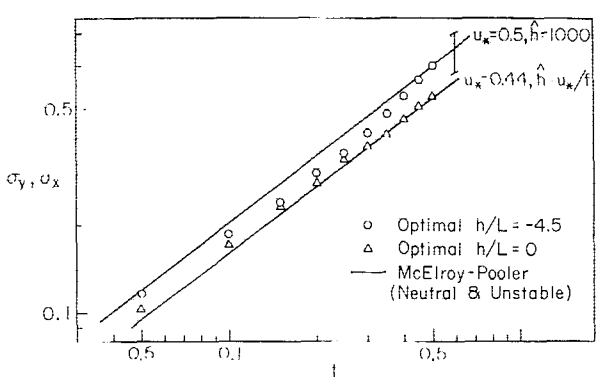

FIG. 13. Optimal streamwise dispersion $\sigma_x(t)$ compared with the empirical lateral dispersion data of McElroy-Pooler.

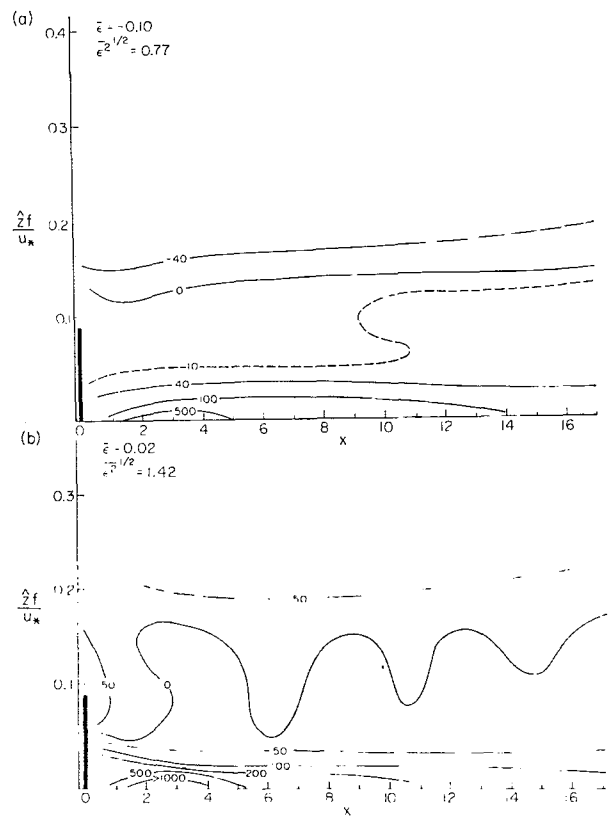

FIG. 15. The fractional error (100ϵ) resulting in (a) the puff model and (b) the plume model using the optimal σ profiles shown in Figs. 12–14 for the neutral case. Errors are relative to the NE concentration distribution given in Fig. 5a.

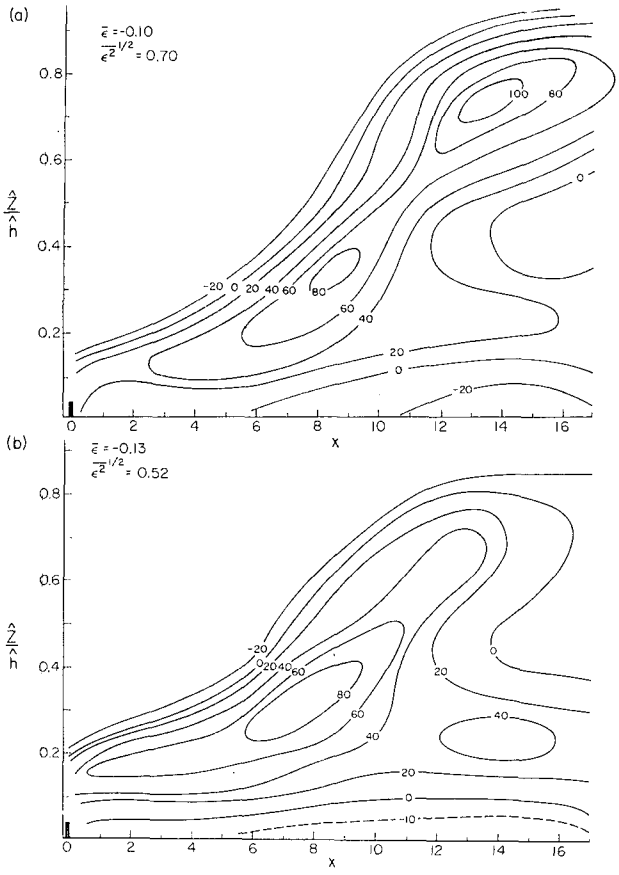

FIG. 16. As in Fig. 15 except for the unstable case ($\hat{h}/L=-4.5$). The corresponding NE solution is shown in Fig. 6a.

The b panels of Figs. 10 and 15 reveal that in using the "optimal" $\sigma_z(x)$ profiles the plume model fails by a considerable margin to achieve the level of accuracy that was attained in the earlier calculations. It will be recalled that in the previous computations the x axis was expanded to account for apparent differences in the mean particle velocities implicit in the empirical data and in the numerical turbulence model. Arbitrary adjustments of the atmospheric stability were also made. By contrast, none of these artifices were employed in computing the optimal $\sigma_z(x)$ values. These facts together with the error values given in Fig. 15b suggest that the basic plume formula does not provide a wholly adequate description of atmospheric diffusion, at least under neutral stability conditions. However, under unstable conditions, the accuracy is greatly improved, as indicated by Fig. 16b.

5. Summary

In the first part of this paper we demonstrated how Lagrangian diffusion theory can be implemented using numerical turbulence models. Through this technique we were able to derive expressions for the distribution of mean concentration of passive material issuing from a continuous point source in the planetary boundary layer. These distributions, shown in Figs. 5a and 6a, have been referred to as the numerico-empirical (NE) solutions of the Lagrangian equation (4). Inasmuch as the data sets on which these solutions were obtained are rather small, the results presented here are only tentative. Future studies will attempt to achieve greater accuracy and will address the important questions of how the concentrations are affected by changes in source height; atmospheric stabilities, other than those treated here; and by changes to other source types, such as area or line sources.

TABLE 2. Optimal parameters for use in the diffusion equation and in the Gaussian puff and plume models (non-dimensional variables).*

Model	Parameter	Stability: Neutral ($\hat{h}/L=0$, $u_*/fz_0=1.5\times10^7$)	Stability: Unstable ($\hat{h}/L=-4.5$, $z_i/z_0=6.8\times10^6$)
Gaussian puff	$\sigma_z(\tau)$	$=0.0045+0.4\tau$, $0.022<\tau\leqslant0.079$ $=0.026+0.129\tau$, $0.079<\tau\leqslant0.32$	$=-0.0023+0.65\tau-1.89\tau^2+5.32\tau^3$, $0.04<\tau\leqslant0.52$
	$\sigma_x(\tau)$	$=1.85\tau$, $0<\tau\leqslant0.045$ $=0.045+0.92\tau$, $0.045<\tau\leqslant0.32$	$=0.045+1.307\tau$, $0.05<\tau\leqslant0.7$
Gaussian plume	$\sigma_z(x)$	$=0.032+0.0044x$, $0.23<x<4.0$	$=0.075+0.0167x$, $0.5<x<5.5$ $=-0.065+0.0435x$, $5.5<x<9.5$
Diffusion equation	$K_Z(z)$	$\approx7.396\times10^{-4}+6.082\times10^{-2}z+2.532z^2-12.72z^3+15.17z^4$, $0<z<0.45$ ≈0, $z>0.45$	$=-6.934\times10^{-3}+0.6113z+3.297z^2-6.442z^3+3.153z^4$, $0.02<z<1.0$
	$\bar{u}(z)$	$=29.82+213.2z-1989z^2+8743z^3-14670z^4$, $0.022<z<0.21$ $=\bar{u}(0.21)$, $z>0.21$	$=26.22+153.2z-1428z^2+5541z^3-7523z^4$, $0.025<z<0.3$ $=\bar{u}(0.3)$, $z>0.3$

* All lengths made nondimensional by the inversion height z_i in unstable case, and by u_*/f in neutral case; times made nondimensional by z_i/u_* (unstable) and $1/f$ (neutral).

Proceeding under the assumption that the accuracies of the present NE solutions are at worst comparable to those of available empirical data, we used these solutions as standards for assessing the accuracies of the three major diffusion models, namely the diffusion equation and the Gaussian puff and plume formulas. Subsequent work was devoted to optimizing the performances of these models. This was done by adjusting the functional forms of the free parameters in each model such that the resulting predictions were in closest overall agreement with the NE solutions. These "optimal" parameters are summarized in functional form in Table 2. Regarding the accuracies of the optimal models, we note the following points.

1) Of the three models, the diffusion equation is by far the superior. Errors are generally of the order of 20% except at points near the source in neutral conditions where much larger discrepancies are observed (see Figs. 5b and 6b).

2) Relative to the plume formula, the Gaussian puff equation is a slightly superior model; but in quantitative terms, neither provides an acceptable description of atmospheric diffusion under neutral stability conditions, at least in the problem considered here. Both models tend to overpredict ground level concentrations arising from elevated sources. Errors of 100% are prevalent and in isolated areas they are much larger. Under unstable conditions the accuracies of the optimal models were acceptable in the problem treated here (see Figs. 15 and 16).

With respect to the Gaussian puff and plume models in general, we note the following points.

1) Spatial concentration distributions in the planetary boundary layer are decidedly nonGaussian.

2) Indications were found here that the Pasquill-Gifford data commonly used in the plume formula are not applicable to emissions from elevated sources unless some allowance is made for wind shear effects. When such modifications were made, we found the accuracy of the plume formula for elevated sources to be greatly improved (see Fig. 10b, as compared with Fig. 15b).

Acknowledgments. R. G. Lamb is indebted to Dr. James Deardorff of the National Center for Atmospheric Research for making available the data from which the particle statistics reported here were computed and for sponsoring a visit to NCAR in the summer of 1971 where these same calculations were performed. This work was supported in part by the National Science Foundation under Grant ENG71-02486, and in part by funds from the Environmental Protection Agency under Grant 68-02-1237.

REFERENCES

Batchelor, G. K., 1949: Diffusion in a field of homogeneous turbulence. Part 1: Eulerian analysis. *Aust. J. Sci. Res.*, **2**, 437–450.

Chen, W. H., and J. H. Seinfeld, 1972: Estimation of spatially varying parameters in partial differential equations. *Intern. J. Control*, **15**, 487–495.

——, G. R. Gavalas, J. H. Seinfeld and M. L. Wasserman, 1974: A new algorithm for automatic history matching. *Soc. Pet. Eng. J.*, **14**, 593.

Corrsin, S., 1959: Progress report on some turbulent diffusion research. *Advances in Geophysics*, Vol. 6, Academic Press, 161–164.

——, 1974: Limitations of gradient transport models in random walks and in turbulence. *Advances in Geophysics*, Vol. 18A, Academic Press, 25–60.

Deardorff, J., 1970: A three-dimensional numerical investigation of the idealized planetary boundary layer. *Geophys. Fluid Dyn.*, **1**, 377–410.

——, 1972: Numerical investigation of neutral and unstable planetary boundary layers. *J. Atmos. Sci.*, **29**, 91–115.

——, and R. L. Peskin, 1970: Lagrangian statistics from numerically integrated turbulent shear flow. *Phys. Fluids*, **13**, 584–595.

Hanjalic, K., and B. E. Launder, 1972: A Reynolds stress model of turbulence and its application to thin shear flows. *J. Fluid Mech.*, **52**, 609–638.

Lamb, R. G., and M. Neiburger, 1971: An interim version of a generalized urban air pollution model. *Atmos. Environ.*, **5**, 239–264.

Lions, J. L., 1971: *Optimal Control of Systems Governed by Partial Differential Equations*. New York, Springer-Verlag, 396 pp.

Lumley, J. L., and B. Khajeh-Nouri, 1974: Computational modeling of turbulent transport. *Advances in Geophysics*, Vol. 18A, Academic Press, 169–192.

McElroy, J. L., 1969: A comparative study of urban and rural dispersion. *J. Appl. Meteor.*, **8**, 19–31.

Monin, A. S., and A. M. Yaglom, 1971: *Statistical Fluid Mechanics*. The MIT Press, 769 pp.

Orszag, S. A., and Y. H. Pao, 1974: Numerical computation of turbulent shear flows. *Advances in Geophysics*, Vol. 18A, Academic Press, 225–236.

Peskin, R. L., 1974: Numerical simulation of Lagrangian turbulent quantities in two and three dimensions. *Advances in Geophysics*, Vol. 18A, Academic Press, 141–163.

Ragland, K. W., 1973: Multiple box model for dispersion of air pollutants from area sources. *Atmos. Environ.*, **7**, 1017–1032.

Riley, J. J., and G. S. Patterson, Jr., 1974: Diffusion experiments with numerically integrated isotropic turbulence. *Phys. Fluids*, **17**, 292–297.

Shir, C. C., and L. J. Shieh, 1974: A generalized urban air pollution model and its application to the study of SO_2 distributions in the St. Louis Metropolitan area. *J. Appl. Meteor.*, **13**, 185–204.

Turner, D. B., 1969: *Workbook of Atmospheric Dispersion Estimates*. U. S. Environmental Protection Agency, Publ. AP-26.